Hindawi
Advances in Materials Science and Engineering
Volume 2017, Article ID 3625414, 8 pages
https://doi.org/10.1155/2017/3625414

Research Article

Activated Carbon Fiber Monoliths as Supercapacitor Electrodes

Gelines Moreno-Fernandez,[1] Joaquin Ibañez,[2] Jose M. Rojo,[1] and Mirko Kunowsky[3]

[1]*Instituto de Ciencia de Materiales de Madrid (ICMM), Consejo Superior de Investigaciones Científicas (CSIC), Sor Juana Inés de la Cruz 3, Cantoblanco, 28049 Madrid, Spain*
[2]*Centro Nacional de Investigaciones Metalúrgicas (CENIM), CSIC, Avda. Gregorio del Amo 8, 28040 Madrid, Spain*
[3]*Inorganic Chemistry Department, University of Alicante, San Vicente del Raspeig S/N, 03080 Alicante, Spain*

Correspondence should be addressed to Mirko Kunowsky; kunowsky@ua.es

Received 31 March 2017; Accepted 30 May 2017; Published 28 June 2017

Academic Editor: Germà Garcia-Belmonte

Activated carbon fibers (ACF) are interesting candidates for electrodes in electrochemical energy storage devices; however, one major drawback for practical application is their low density. In the present work, monoliths were synthesized from two different ACFs, reaching 3 times higher densities than the original ACFs' apparent densities. The porosity of the monoliths was only slightly decreased with respect to the pristine ACFs, the employed PVDC binder developing additional porosity upon carbonization. The ACF monoliths are essentially microporous and reach BET surface areas of up to 1838 $m^2\ g^{-1}$. SEM analysis reveals that the ACFs are well embedded into the monolith structure and that their length was significantly reduced due to the monolith preparation process. The carbonized monoliths were studied as supercapacitor electrodes in two- and three-electrode cells having 2 M H_2SO_4 as electrolyte. Maximum capacitances of around 200 F g^{-1} were reached. The results confirm that the capacitance of the bisulfate anions essentially originates from the double layer, while hydronium cations contribute with a mixture of both, double layer capacitance and pseudocapacitance.

1. Introduction

Supercapacitors (such as electric double layer capacitors, EDLC) are electrochemical energy storage devices that typically provide energy densities which are higher than conventional capacitors, but lower than batteries. Furthermore, they feature high power densities, fast charging capabilities, and long cycle lives, amongst other things. These characteristics make them interesting candidates for a number of applications, for example, in electronic devices, smart grids, or hybrid and electric vehicles [1]. The principal elements of supercapacitors are their electrodes and electrolytes at which interfaces charges are stored, either through separation (double layer capacitance) or through reversible redox reactions (pseudocapacitance). Due to the requirements of the electrode materials, such as high amounts of suitable and accessible porosity, high electric conductivities, and high densities (in order to reduce the size of the device), carbons are amongst the most investigated materials.

Carbon fibers are well known for their mechanical properties, combining high tensile strength with light weight [2, 3]. In the case of carbon activation, carbon fibers are interesting precursors, because their fibrous structure (i) is very homogeneous and well-defined, ensuring high reproducibility, (ii) is beneficial for developing directly accessible microporosity, and (iii) provides higher adsorption rates [4–6]. Due to these characteristics, as well as the good electric conductivities along their fiber axis, activated carbon fibers (ACF) are promising alternatives as supercapacitor electrode materials [7–15].

Activated carbon fibers usually have relatively low apparent densities (referring to a volume occupied without any compression). Due to their fibrous shapes and lengths this volume is relatively large and can be significantly decreased (thus, augmenting the density) by applying a mechanical pressure. However, the fiber's resilience causes that to a certain extend the material tends to return to its initial state [16]. Such behavior can be counterproductive for some kinds

of applications in which the available space is limited, for example, in gas storage applications, where storage vessels occupy a determined volume [17, 18]. Furthermore, in the case of electrochemical energy storage applications, also electric characteristics such as the electric conductivity are affected by this behavior. Thus, from a practical point of view, it is of much interest to produce materials from activated carbon fibers, such as monoliths, which are able to preserve the shape of the compressed fibers under working conditions, have high densities, and are easy to handle.

Recently, we investigated monoliths from activated anthracite, synthesized using PVDC binder, as supercapacitor electrodes, obtaining promising results [19]. In the present work, this research is extended to activated carbon fiber monoliths.

2. Materials and Experimental Methods

2.1. Activated Carbon Fibers (ACF). The two activated carbon fibers (ACF) that were used as precursors for the monoliths were kindly provided by Nippon Kynol Inc. (Gun-Ei Chemical Industry Co., Ltd., Japan) and comprise Kynol ACF-1603-15 and Kynol ACF-1603-25. These ACFs (here-after identified as ACF15 and ACF25) were produced from a phenolic resin (novoloid).

2.2. ACF Monolith Preparation. The monoliths were prepared by mixing the ACFs with distilled water and then adding a 55% aqueous solution of polyvinylidene chloride (PVDC) (Waterlink Sutcliffe Carbons, UK) which was used as a binder. For drying, the PVDC/ACF mixture was heated to 363 K, keeping this temperature constant for 24 h. Afterwards, the dry mixture was ground and introduced into a cylindrical piston mold of a mechanical press. Here, the mixture was progressively exposed to increasing pressures, until reaching a maximum pressure of 259 N mm^{-2}. While being exposed to this pressure, the mixture was heated up to 413 K and, upon reaching this temperature, cooled down by convection obtaining PVDC/ACF monoliths. In order to carbonize the PVDC binder, the monoliths were slowly (heating rate: 2 K min^{-1}) and stepwise (constant heating steps at 448 K and 723 K for 1 hour each and at 1023 K for 2 hours) heated in a horizontal tube furnace under a N_2 flow of 100 ml min^{-1}. Subsequently, the furnace was switched off and cooled down by convection. In the case of both ACF precursors (ACF15 and ACF25), the PVDC/ACF ratio was 1/1 (weight basis), resulting in the all-carbon monoliths ACF15-M and ACF25-M, respectively.

2.3. Porosity Characterization. Subatmospheric gas adsorption measurements of nitrogen at 77 K and of carbon dioxide at 273 K were carried out in a Quantachrome Autosorb 6. Prior to the adsorption measurements, the samples were degassed at 523 K for 4 hours under vacuum. In order to get representative samples, the monoliths were crashed and grounded, before their porosity characterization. The specific BET surface areas (S_{BET}) were calculated, and the total micropore volumes ($V_{DR}(N_2)$) of pores smaller than 2 nm and narrow micropore volumes ($V_{DR}(CO_2)$) of pores smaller than 0.7 nm were obtained from N_2- and CO_2-adsorption isotherms, respectively, and using the Dubinin-Radushkevich (DR) equation. Nonlinear Density Function Theory (NLDFT) pore size distributions were calculated, using the standard carbon slit pore model and were performed without regularization (lambda = 0).

2.4. SEM. The microstructural characterization of the monoliths was performed by scanning electron microscopy (SEM) equipped with energy dispersive X-ray spectroscopy (EDS) in a FEG HITACHI S-4800 instrument. The pristine fibers were analyzed in a Hitachi S-3000N. Prior to the analysis, the samples were supported on a conductive tape. In addition, the carbon monoliths were also embedded in a resin and prepared by standard metallographic techniques. The images were obtained in the backscattered electron (BSE) mode or in the secondary electron (SE) mode.

2.5. Density. Apparent densities of the activated carbon fibers were measured, taking into account the weight of the degassed fibers and the volume occupied by the loose sample, without applying any compacting pressure. The density of the monoliths was deduced from their weight after degasification and from their geometric dimensions, measuring their diameters and heights using a caliper rule.

2.6. Mechanical Measurements. Three-point bending tests were performed in a conventional 10T-SERVOSIS machine, in order to study the mechanical properties of the monoliths. The ACF monolith samples had ca. 10 mm in length, 5 mm width, and 4 mm thickness. The span length, that is, the distance between the two supports, was 7 mm. The cross-head speed was 0.005 mm s^{-1}. Stress (σ) and strain (ε) were calculated according to the equations: $\sigma = 3 \cdot F \cdot l/(2 \cdot w \cdot h^2)$ and $\varepsilon = 6 \cdot h \cdot \delta/(l \cdot 2)$, respectively, where F is the load, l is the span length, w is the monolith width, h is the monolith thickness, and δ is the deflection increment.

2.7. Electrochemical Measurements. The electrochemical measurements were performed in aqueous 2 M H_2SO_4 electrolyte. In order to characterize the monoliths as electrodes, parallelepipedic pieces of approximately 50 mg in weight and dimensions 11 × 5 × 2 mm^3 were obtained from the starting monoliths. Prior to the electrochemical measurements, the monoliths were immersed into the electrolyte and infiltrated under primary vacuum (ca. 10^{-1} Torr) for 2 days. In the case of the symmetric two-electrode cells, two equal monoliths were separated by a glassy microfiber paper (Whatman 934 AH) in Swagelok-type cells. In the case of three-electrode cells, the monolith was used as the working electrode, Hg/Hg_2SO_4 was used as the reference electrode, and Pt wire was used as the counter electrode.

3. Results and Discussion

3.1. Porosity and Mechanical Properties. In Table 1, the porous characteristics of the investigated materials are outlined. Concerning the pristine activated carbon fibers, it can be seen that ACF25 has a higher porosity than ACF15. Thus,

Table 1: Results from porosity characterization.

Sample	S_{BET} ($m^2\,g^{-1}$)	V_{DR} (N_2) ($cm^3\,g^{-1}$)	V_{DR} (CO_2) ($cm^3\,g^{-1}$)	Density ($g\,cm^{-3}$)
ACF15	1176	0.55	0.52	0.24
ACF25	1989	0.87	0.62	0.17
ACF15-M	1127	0.52	0.41	0.69
ACF25-M	1838	0.78	0.55	0.54

the specific BET surface areas of ACF25 and ACF15 are 1989 and 1176 $m^2\,g^{-1}$, their total micropore volumes (of pores < 2 nm) are 0.87 and 0.55 $cm^3\,g^{-1}$, and their narrow micropore volumes (of pores < 0.7 nm) are 0.62 and 0.52 $cm^3\,g^{-1}$, respectively. In turn, ACF15 has a higher density (0.24 $g\,cm^{-3}$) than ACF25 (0.17 $g\,cm^{-3}$). It has to be pointed out that in the case of the pristine activated carbon fibers the density values correspond to apparent densities. Under mechanical pressure, these values can be significantly improved (more than 2.5 times); however, the fibers are resilient and tend to spring back when the applied pressure is removed, limiting their practical density [16].

Monoliths were successfully synthesized from both activated carbon fibers with PVDC as a binder, using a PVDC/fiber weight ratio of 1/1 in both cases. The N_2-adsorption isotherms in Figure 1(b) are of type I, according to the IUPAC definition, indicating that the monoliths are essentially microporous [20]. Thus, both isotherms adsorb most of the nitrogen at very low relative pressures and reveal a steep increase at the onset. The steep increase opens out into a "knee"-region where the adsorption rate is progressively truncated which, in turn, concludes in a flat, almost horizontal, curve progression that marks the maximum adsorption amount at the end of its course at relative pressure 1. It can be observed that ACF15-M has a much narrower knee-region than ACF25-M, indicating that its porosity is more restricted to narrow micropores. On the other hand, ACF25-M reaches a higher maximum adsorption amount, thus, identifying a higher overall porosity. The CO_2-adsorption isotherms in Figure 1(c) disclose that ACF15-M reaches insignificantly higher values during the first third of the isotherm than ACF25-M. Afterwards, the adsorption rate of ACF15-M abates stronger than the one of ACF25-M, so that the latter monolith reaches around 10% more maximum CO_2-adsorption at $P/P_0 = 0.03$. The observations are confirmed by the porosity values disclosed in Table 1. Hence, ACF25-M reaches higher porosity values than ACF15-M, with BET surface areas of 1838 and 1127 $m^2\,g^{-1}$, total micropore volumes of 0.78 and 0.52 $cm^3\,g^{-1}$, and narrow micropore volumes of 0.55 and 0.41 $cm^3\,g^{-1}$, respectively. Interestingly, these values are only slightly lower than the values of the pristine activated carbon fibers. This is due to two circumstances: On the one hand, the added PVDC binder decomposes during the carbonization process step, leaving a residual amount of carbon which is around 20% of the initial amount of PVDC [16, 19]. On the other hand, additional porosity is generated upon PVDC decomposition, so that the residual amount of carbon originating from it reaches a BET surface area of around 580 $m^2\,g^1$ [19]. Therefore, two porous carbon phases are present in the finished monoliths: the activated carbon fibers and the porous carbon phase that stems from the carbonized PVDC. When the rule of mixtures is applied, taking into account the phase amounts and the BET surface areas of each of them, the calculated values are in good agreement with the experimental ones, within an error of around 5% for both monoliths. It has to be highlighted that, aside from the only marginal porosity loss, the density of the monoliths is significantly increased. Thus, the densities accomplished by the monoliths (0.69 $g\,cm^{-3}$ for ACF15-M and 0.54 $g\,cm^{-3}$ for ACF25-M, resp.) are around three times higher than the apparent densities of the pristine activated carbon fibers. The results from three-point bending tests are shown in Figure 1(c), the plots having shapes that are characteristic for brittle materials. The two monoliths reveal quite different mechanical properties. Thus, ACF25-M only reaches a maximum stress value of less than 0.5 MPa, while the stress value of ACF15-M is around 8 times higher (close to 4 MPa). This indicates either that the strength of the pristine ACF-15 fiber is significantly higher than for ACF-25, or that the integration of the pristine fiber into the monolith structure is better for ACF15-M than for ACF25-M. When compared with activated anthracite monoliths with similar PVDC/precursor ratios, lower values are obtained with the present ACF monoliths [19].

The NLDFT pore size distribution and the cumulative pore volume diagram are represented in Figures 1(d) and 1(e), respectively. The plots confirm the observations made for the adsorption isotherms. Thus, both monoliths are essentially microporous, the major peaks being around 0.9 to 1.2 nm. In the case of ACF25-M this peak represents around 40% of its total porosity, while it is around 90% in the case of ACF15-M. Thus, the NLDFT diagrams confirm that the porosity of ACF15-M is more restricted to micropores. In fact, the pores of ACF15-M are entirely smaller than 2 nm, while in the case of ACF25-M a minor portion of the pores are supermicropores between 2 and 3 nm. Interestingly, the major peak of ACF25-M is slightly shifted to smaller pores, and a small additional peak can be found for pores of ca. 0.5 nm.

3.2. SEM. SEM images of the investigated materials are depicted in Figure 2. Figures 2(a) and 2(b) illustrate low resolution images of the pristine activated carbon fibers ACF15 and ACF25, respectively. It can be observed that both fibers have very similar structures with typical lengths of more than 1 mm and diameters of around 10 μm. In Figures 2(c) and 2(e), the monolith ACF25-M and, in Figures 2(d) and 2(f), the monolith ACF15-M are depicted in secondary electron mode (SE). In the case of both monoliths, two different phases can be distinguished: On the one hand the

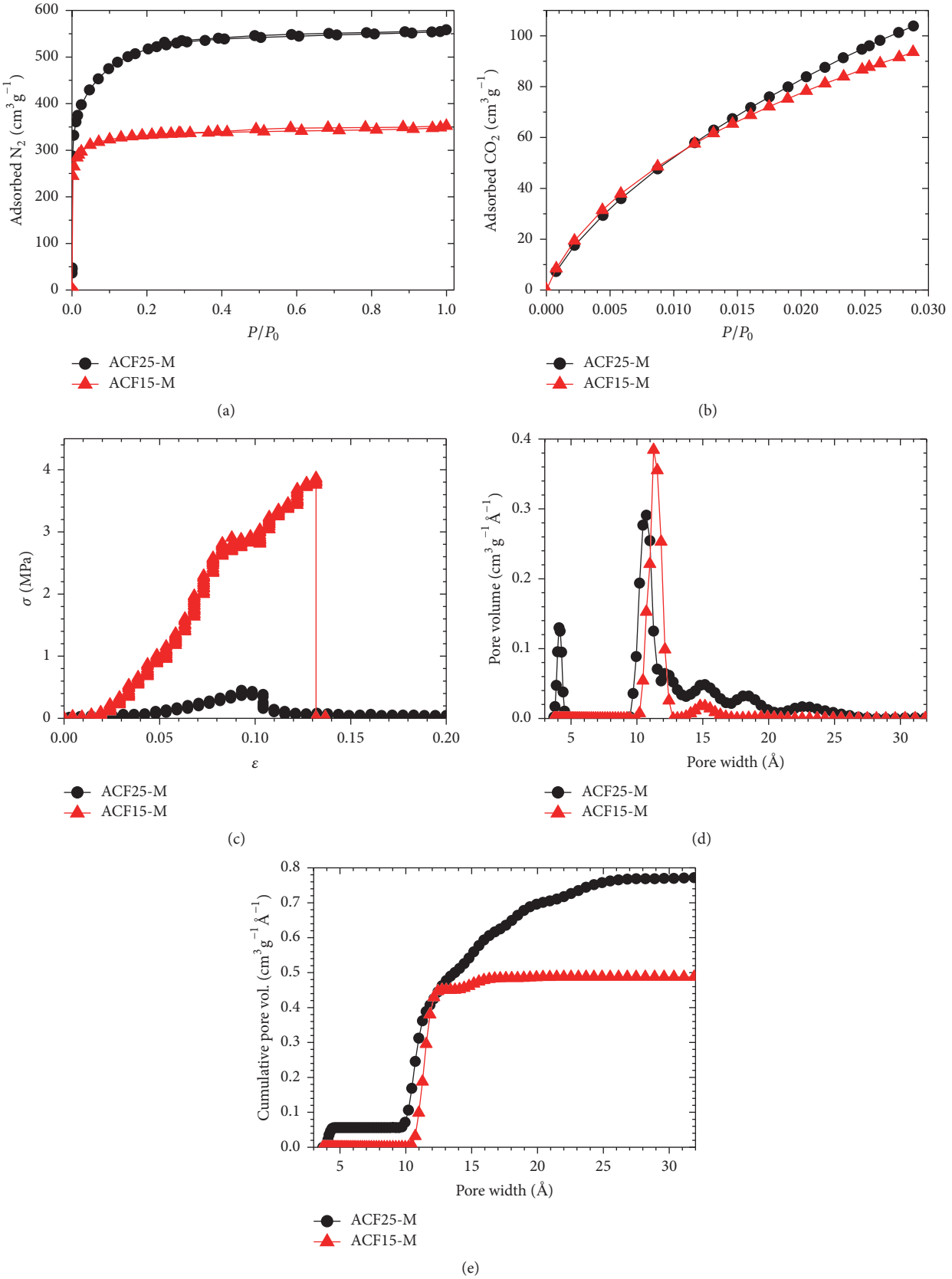

Figure 1: (a) Nitrogen adsorption isotherms obtained at 77 K; (b) carbon dioxide adsorption isotherms obtained at 273 K; (c) mechanical properties from three-point bending tests, represented as stress σ versus strain ε; (d) NLDFT pore size distribution obtained from the N_2 adsorption data; and (e) cumulative pore size distribution.

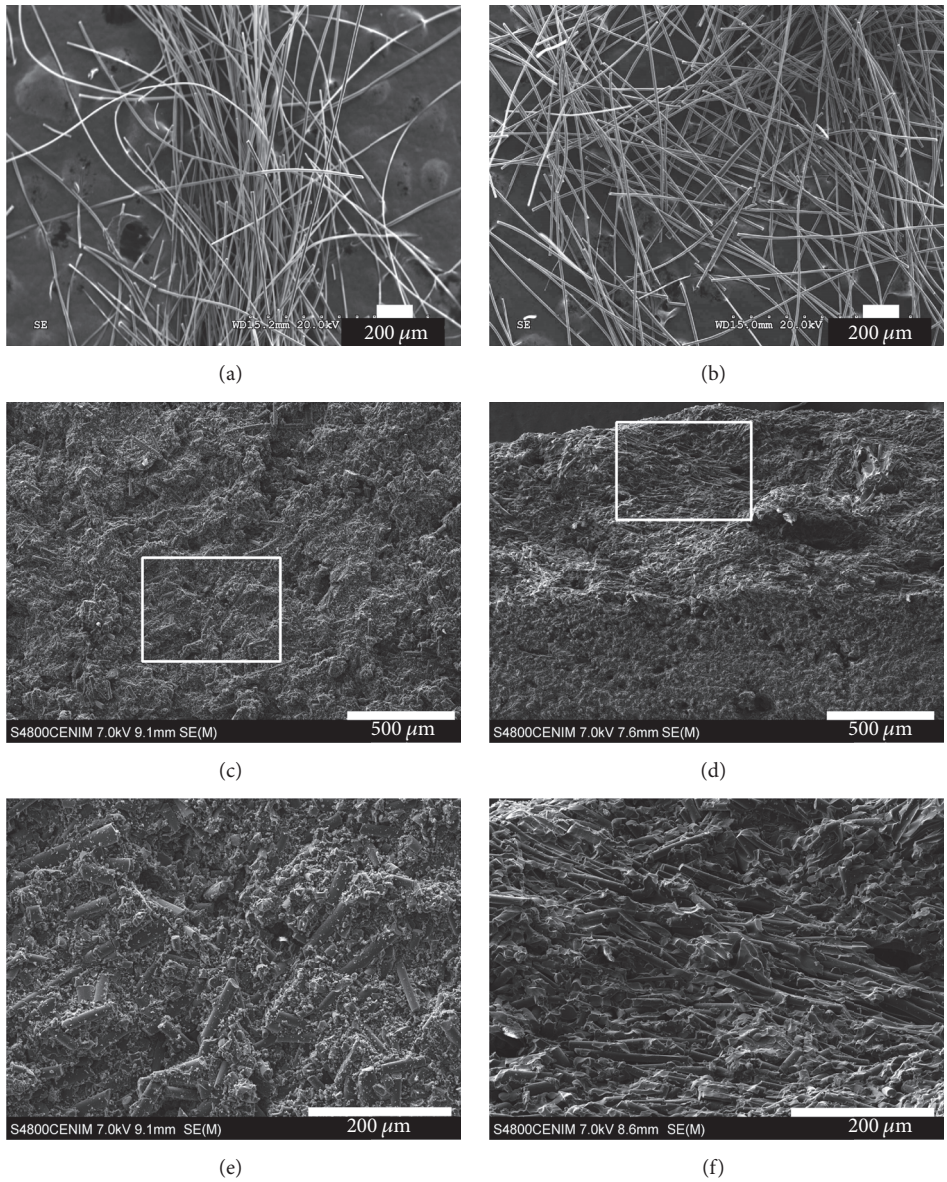

Figure 2: SEM images of the pristine activated carbon fibers (a) ACF15 and (b) ACF25; low resolution SEM images of the ACF monoliths (c) ACF15-M and (d) ACF25-M, the white squares indicating the enlarged areas shown in high resolution SEM images of (e) ACF15-M and (f) ACF25-M, respectively.

carbonized PVDC binder and on the other hand the activated carbon fibers as well as fractures thereof. Microanalysis revealed only traces of chlorine (around 0.1 at.%), indicating that the PVDC binder was thoroughly carbonized. When compared with the images of the pristine activated carbon fibers in Figures 2(a) and 2(b), it is important to note that the length of the fibers in the monoliths is significantly reduced. This indicates that the fibers suffered from the mechanical treatments along with the monolith preparation process, for example, concerning the grinding of the dried mixture and the pressurization step in the mechanical press. Another observation from Figures 2(c)–2(f) is that the fibers are well embedded into the carbonized binder, so that both carbon phases form the integrated structure of the monoliths.

The higher magnification of polished monolith samples (not shown) allows for better observation of the interface between the activated carbon fibers and the carbonized binder and confirms the good integration of the activated carbon fibers into the matrix. A good form-closed contact between both phases is crucial for achieving suitable electric conductivities, avoiding islanding of electrically isolated and, thus, preventing electrochemically inactive regions.

3.3. Electrochemistry. The dependence of the total specific capacitance measured in two-electrode cells, $C_{total,2E}$, as a function of the current density is shown in Figure 3(a). $C_{total,2E}$ reaches maximum values of 140 F g^{-1} and 203 F g^{-1} for ACF15-M and ACF25-M, respectively (see Table 2), which

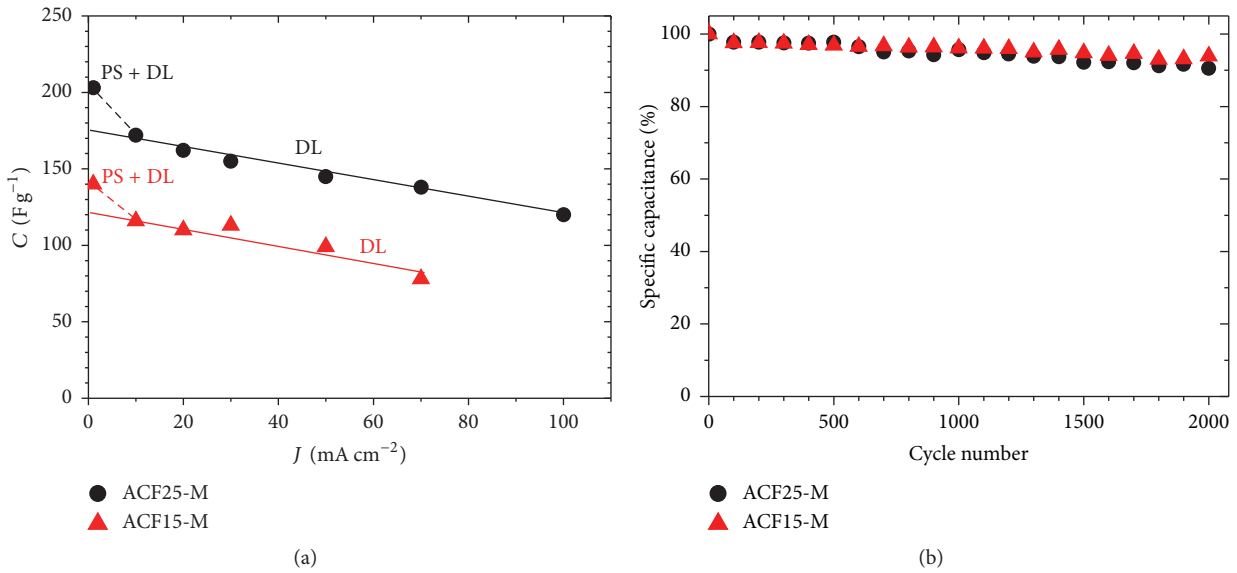

Figure 3: Electrochemical results obtained with two-electrode cells for the two monoliths ACF15-M and ACF25-M: (a) total specific capacitance versus current density; (b) dependence of the specific capacitance as a function of the cycle number at a current density of 40 mA cm^{-2}.

are similar or even higher than the values reported for other activated carbon fibers in aqueous electrolytes [9–15]. In Figure 3(a), it can be observed that the total specific capacitance slightly decreases as the current density increases, showing high capacitance retention for both monoliths. In a previous study, monoliths were synthesized employing a similar preparation procedure with PVDC binder, however, using KOH-activated anthracite instead of activated carbon fibers [19]. Extrapolations of capacitances as J→0 (see straight lines in Figure 3(a)) corresponded to the capacitances of the double layer [19]. Thus, as a rough estimate, double layer capacitance values ($C_{DL,2E}$) of around 121 F g^{-1} and 175 F g^{-1} (both 86%) are attained by ACF15-M and ACF25-M, respectively. The difference between $C_{total,2E}$ and $C_{DL,2E}$ gives values of 19 F g^{-1} and 28 F g^{-1}, which correspond in a first approximation to the pseudocapacitances ($C_{PS,2E}$) of ACF15-M and ACF25-M, respectively. When the total capacitance is expressed in volumetric terms (C_v), a maximum value of 110 F cm^{-3} is achieved by the ACF25-M monolith. Although the ACF15-M monolith has a lower porosity and, thus, a lower specific total capacitance, its volumetric total capacitance is only slightly lower (97 F cm^{-3}), thanks to its higher density.

In Figure 3(b), the cyclability results are shown for both monoliths, ACF15-M and ACF25-M. The measurements were performed in the two-electrode cell configuration and using current densities of 40 mA cm^{-2}. It can be observed that, up to 2000 charging-discharging cycles, the capacitance retention is similar and rather high for both monoliths (above 90%).

In addition to the experiments in two-electrode configuration, measurements in a three-electrode cell were performed for the ACF25-M monolith. The cyclic voltammetry (CV) recorded at 0.1 mV s^{-1} is represented in Figure 4(a). The significant increases in intensity at the negative and positive potential extremes are associated with water decomposition, causing hydrogen evolution at the negative and oxygen evolution at the positive end. The CV reveals an essentially rectangular shape, confirming the high contribution of the double layer capacitance to the total capacitance. A broad peak at around −0.3 V indicates the small pseudocapacitance contribution associated with the hydronium ion.

The galvanostatic charge/discharge plots in Figure 4(b) were recorded at 1 mA cm^{-2} (nearly steady state) and show linear dependence (straight blue lines) in the total voltage range from −0.7 to 0.2 V. In this range, the total specific capacitance was determined according to

$$C_{total,3E} = I \cdot \frac{t_d}{(\Delta V \cdot m)}, \quad (1)$$

where I is the applied current, t_d is the discharge time, ΔV is the voltage range, and m is the electrode weight. The total specific capacitance, reaching 206 F g^{-1}, agrees with the value obtained from measurements in the two-electrode cell, of 203 F g^{-1}.

Moreover, measurements in the three-electrode configuration permit separating the specific capacitance associated with the hydronium cations from that of the bisulfate anions. Figures 4(c) and 4(d) show the galvanostatic plots obtained for the ACF25-M monolith at 1 mA cm^{-2} in the two voltage ranges, $\Delta V(H_3O^+)$ from the open circuit potential (OCP) to negative voltages and $\Delta V(HSO_4^-)$ from the OCP to positive voltages. The specific capacitances associated with the two types of ions were calculated using (1). The specific capacitance measured for the bisulfate ion, $C(HSO_4^-)$ = 173 F g^{-1}, is entirely attributed to a double layer capacitance (see Figure 4(d)). However, the specific capacitance measured for the hydronium ion, $C(H_3O^+)$ = 212 F g^{-1}, contains a pseudocapacitive contribution, in addition to its double layer capacitance. The presence of the two contributions explains

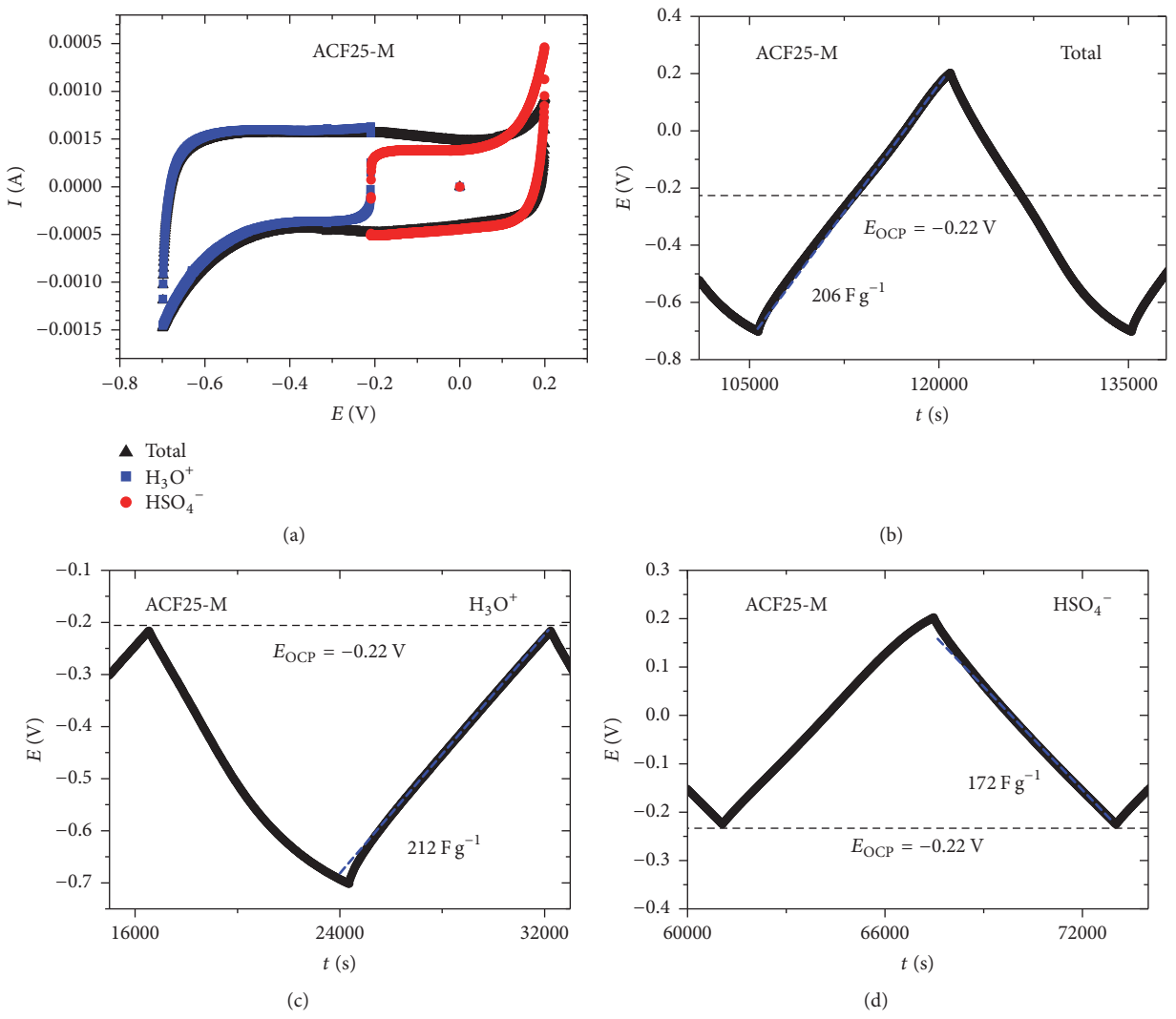

Figure 4: Electrochemical results obtained with three-electrode cells for the monolith ACF25-M: (a) cyclic voltammetry recorded at 0.1 mV s^{-1} in the total voltage range and in the voltage ranges for H_3O^+ and HSO_4^-; (b-d) galvanostatic plots obtained at 1 mA cm^{-2}: (b) for both ions in the total voltage range; (c) for the hydronium ion; and (d) for the bisulfate ion.

Table 2: Results from electrochemical characterization.

Sample	$C_{total,2E}$ (F g^{-1})	$C_{DL,2E}$ (F g^{-1})	$C_{PS,2E}$ (F g^{-1})	$C_{total,3E}$ (F g^{-1})	C_v (F cm^{-3})
ACF15-M	140	121	19	—	97
ACF25-M	203	175	28	206	110

the higher value found for $C(H_3O^+)$ as compared with $C(HSO_4^-)$.

4. Conclusions

Monoliths from activated carbon fibers (ACFs) were used as electrodes in supercapacitors. When compared with the pristine activated carbon fibers, the essentially microporous ACF monoliths only loose relatively few porosity; in turn, their density is around 3-fold the apparent density of the fibers. The length of the fibers suffers considerably from the monolith preparation process; however, the ACFs are found to be well-integrated into the structure of the monoliths. The ACF monoliths reach total capacitances of more than 200 F g^{-1} with relatively high double layer contributions (86% of total capacitance). These results were confirmed by complementary two- and three-electrode cell measurements. Furthermore, the bisulfate anions solely provide double layer capacitance, while the hydronium cations deliver both, double layer capacitance and pseudocapacitance.

Conflicts of Interest

The authors declare that there are no conflicts of interest regarding the publication of this paper.

Acknowledgments

Professor A. Linares-Solano, now retired, is deeply acknowledged for helpful discussions about preparation of carbon monoliths, activation, and porosity. Financial support through the projects of reference MAT2014-57687-R, GV/FEDER (PROMETEOII/2014/010), and University of Alicante (VIGROB-136) is gratefully acknowledged. Edurne Laurín is acknowledged for the preparation of SEM samples.

References

[1] A. Yu, V. Chabot, and J. Zhang, *Electrochemical Supercapacitors for Energy Storage and Delivery Fundamentals and Applications*, Taylor & Francis, Boca Raton, Fla, USA, 2013.

[2] L. H. Peebles, *Carbon Fibers: Formation, Structure, and Properties*, CRC Press, Boca Raton, Fla, USA, 1995.

[3] J.-B. Donnet Marcel Dekker, New York, NY, USA, 1998.

[4] M. Suzuki, "Activated carbon fiber: fundamentals and applications," *Carbon*, vol. 32, no. 4, pp. 577–586, 1994.

[5] M. Inagaki, *New Carbons: Control of Structure And Functions*, Elsevier Science, New York, NY, USA, 2000.

[6] E. J. Bottani and J. M. D. Tascón, *Adsorption by Carbons*, Elsevier, Burlington, NJ, USA, 2008.

[7] J. F. Snyder, E. L. Wong, and C. W. Hubbard, "Evaluation of commercially available carbon fibers, fabrics, and papers for potential use in multifunctional energy storage applications," *Journal of the Electrochemical Society*, vol. 156, no. 3, pp. A215–A224, 2009.

[8] S. Hu, S. Zhang, N. Pan, and Y.-L. Hsieh, "High energy density supercapacitors from lignin derived submicron activated carbon fibers in aqueous electrolytes," *Journal of Power Sources*, vol. 270, pp. 106–112, 2014.

[9] K. Leitner, A. Lerf, M. Winter et al., "Nomex-derived activated carbon fibers as electrode materials in carbon based supercapacitors," *Journal of Power Sources*, vol. 153, no. 2, pp. 419–423, 2006.

[10] J.-H. Lin, T.-H. Ko, Y.-H. Lin, and C.-K. Pan, "Various treated conditions to prepare porous activated carbon fiber for application in supercapacitor electrodes," *Energy and Fuels*, vol. 23, no. 9, pp. 4668–4677, 2009.

[11] H. Qian, H. Diao, N. Shirshova et al., "Activation of structural carbon fibres for potential applications in multifunctional structural supercapacitors," *Journal of Colloid and Interface Science*, vol. 395, no. 1, pp. 241–248, 2013.

[12] Z. Jin, X. Yan, Y. Yu, and G. Zhao, "Sustainable activated carbon fibers from liquefied wood with controllable porosity for high-performance supercapacitors," *Journal of Materials Chemistry A*, vol. 2, no. 30, pp. 11706–11715, 2014.

[13] L. Dong, C. Xu, Q. Yang, J. Fang, Y. Li, and F. Kang, "High-performance compressible supercapacitors based on functionally synergic multiscale carbon composite textiles," *Journal of Materials Chemistry A*, vol. 3, no. 8, pp. 4729–4737, 2015.

[14] S. I. Abd Razak, I. F. Wahab, F. Fadil, F. N. Dahli, A. Z. Md Khudzari, and H. Adeli, "A review of electrospun conductive polyaniline based nanofiber composites and blends: processing features, applications, and future directions," *Advances in Materials Science and Engineering*, vol. 2015, Article ID 356286, 19 pages, 2015.

[15] D. M. Mijailović, M. M. Vukčević, Z. M. Stević et al., "Supercapacitive performances of activated highly microporous natural carbon macrofibers," *Journal of The Electrochemical Society*, vol. 164, no. 6, pp. A1061–A1068, 2017.

[16] M. Kunowsky, J. P. Marco-Lozar, and Á. Linares-Solano, "Activated carbon fibre monoliths for hydrogen storage," *Advances in Science and Technology*, vol. 93, pp. 102–111, 2014.

[17] F. D. Lamari, B. Weinberger, M. Kunowsky, and D. Levesque, "Material design using molecular modeling for hydrogen storage," *AIChE Journal*, vol. 55, no. 2, pp. 538–547, 2009.

[18] J. P. Marco-Lozar, M. Kunowsky, J. D. Carruthers, and Á. Linares-Solano, "Gas storage scale-up at room temperature on high density carbon materials," *Carbon*, vol. 76, pp. 123–132, 2014.

[19] G. Moreno-Fernandez, M. Kunowsky, M. Á. Lillo-Ródenas, J. Ibañez, and J. M. Rojo, "New carbon monoliths for supercapacitor electrodes. Looking at the double layer," *ChemElectroChem*, vol. 4, no. 5, pp. 1016–1025, 2017.

[20] M. Thommes, K. Kaneko, A. V. Neimark et al., "Physisorption of gases, with special reference to the evaluation of surface area and pore size distribution (IUPAC Technical Report)," *Pure and Applied Chemistry*, vol. 87, no. 9-10, pp. 1051–1069, 2015.